SAND2008-4769C

Title: *Mode II Fracture – Simulations and Experiments*

Authors: Arthur Brown
Wei-Yang Lu
James Foulk III
Stephen Margolis
Thomas Bennett
Yuki Ohashi

ABSTRACT

We have utilized cohesive zone models in Sandia's quasistatics finite-element code, Adagio, to model mode II failure along bonded interfaces. End-notched flexure (ENF) experiments were conducted using bimaterial composite specimens. Finite-element simulations were performed that agreed well with the experimental results. The simulations included the effects of thermal mismatch by modeling the cool-down from the cure temperature to room temperature before loading is applied.

Adagio and the DAKOTA software toolkit were used to perform a sensitivity analysis study of the ENF simulation parameters. The material test specimen was characterized using 37 uncertain geometric and material property parameters, each having a range of +/-5% its nominal value. DAKOTA's Latin Hypercube Sampling method was used to generate an ensemble of 800 Adagio simulations, from which maximum load and compliance responses of the test specimen were computed. Linear and quadratic model fits were performed for each of the response functions. The sensitivity of each parameter was determined based on a statistical test for a null hypothesis, to check whether or not the coefficient of the corresponding term in the model fit, normalized by its standard deviation, is sufficiently close to zero.

Follow-on uncertainty quantification studies using Adagio and DAKOTA will be performed in the future. Temperature and rate effects are also being studied, and experiments with mode I and mixed-mode failure will be conducted.

Sandia National Laboratories, MS9042, Livermore, CA 94551-0969, U.S.A.

INTRODUCTION

Composite materials are prominent in many applications, such as aircraft, fuel tanks, and wind turbine blades. One of the types of failure that can be found in composite structures is delamination between plies under normal and/or shear stresses. For this reason, the determination of the critical energy release rate is crucial to analyze designs. Typical methods of determining the critical energy release rate are through experiments, such as the double-cantilever beam (DCB) for mode I, end-notched flexure (ENF) for mode II, and mixed-mode flexure (MMF) for mixed mode.

Mode-II delamination has been modeled by a number of authors. Most use symmetric, single-material ENF geometries (see e.g. de Moura [1], Iannucci [2], and Mi et al. [3]). Liu et al. [4] used a bimaterial ENF specimen, and compared ADCB simulations to experimental results, but no comparison between experiment and analysis was made for the ENF geometry.

In this paper, ENF experiments are performed on bimaterial composite specimens that were cured at an elevated temperature. It is found that the residual stresses in the specimens after curing play a key role in determining the failure load. Finite-element simulations are presented that model delamination at the interface between two composite materials using the cohesive zone model of Tvergaard and Hutchinson [5]. In the first section, experiments are described that are used to determine the bulk properties of the composite materials. Next, mode-II experimental results for the ENF geometry are given, as well as the simulation responses. Sensitivity analysis is then performed to see which parameters have the greatest impact on two response functions.

EXPERIMENTS

Bulk Testing

The orthotropic material properties for the 3k, woven E-glass (Hexcel 7781, 8-harness satin weave with a UF3362 TCR resin system) and 1k graphite (Toray T-300, 5-harness satin weave with a UF3360 TCR resin system) composite layers were determined using a combination of experimental results, micromechanics, and engineering judgment. For each composite material, tensile specimens were manufactured with three different orientations: 0°, 45°, and 90° off the rolling axis (see Figure 1). Each specimen consisted of five plies. All specimens were fabricated with Teflon-coated peel-ply and cured at 350 °F for one hour at 45 psi (see Figure 2). Additional panels were fabricated to obtain the fiber volume fraction. The resulting fiber volume fractions were 60% for graphite and 66% for E-glass, as measured using Archimedes' method with a stack of four specimens (0.75 in by 0.75 in) in ethanol to obtain proper wetting.

The 0° and 90° specimens were used to determine Young's moduli and Poisson's ratios (see ASTM D3039-76 in [7]), and the 45° specimens were used to calculate the in-plane shear moduli (see ASTM D3518 in [7]). An example of the specimen response is shown in Figure 3. For each material and material orientation,

specimens were loaded and unloaded elastically multiple times at room temperature. The axial and transverse strains were measured with a strain gage (type CEA-06-250UT-350) mounted in the center of the gauge section (see Figure 1). The resulting property sets are shown in Table 1, where the notation 11 refers to the 0° direction, 22 is the 90° direction, and 33 is the out-of-plane direction. The measurements of the moduli were taken at the beginning of the third loading cycle. For each material and material orientation, three specimens were tested, and each was tested three times, for a total of nine measurements taken for each material property. Standard deviations for the measured moduli were less than 1% of the mean values.

The values of some of the bulk properties were estimated instead of experimentally determined due to the time and cost constraints. The purpose of the sensitivity analysis performed later in this paper was in part to see if these parameters have a significant impact on the results, and if so, then to perform additional experiments to determine the values more accurately.

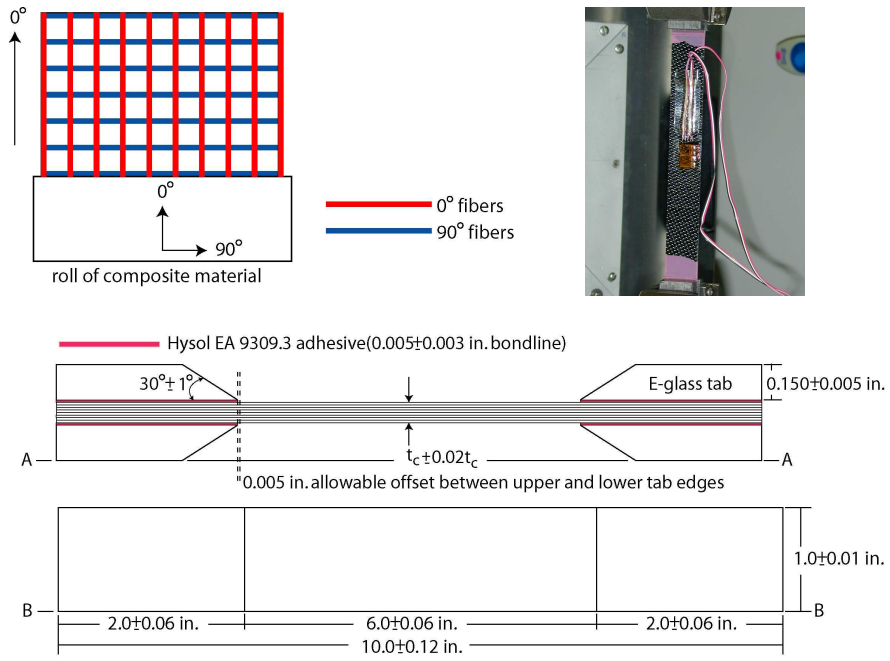

Figure 1. Composite tensile specimen design.

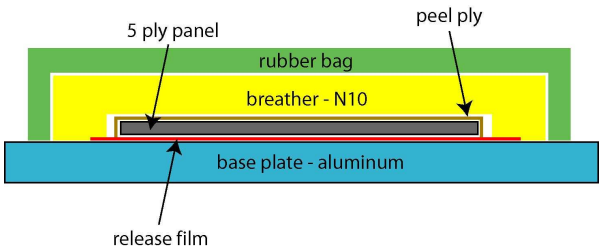

Figure 2. Fabrication of composite specimens.

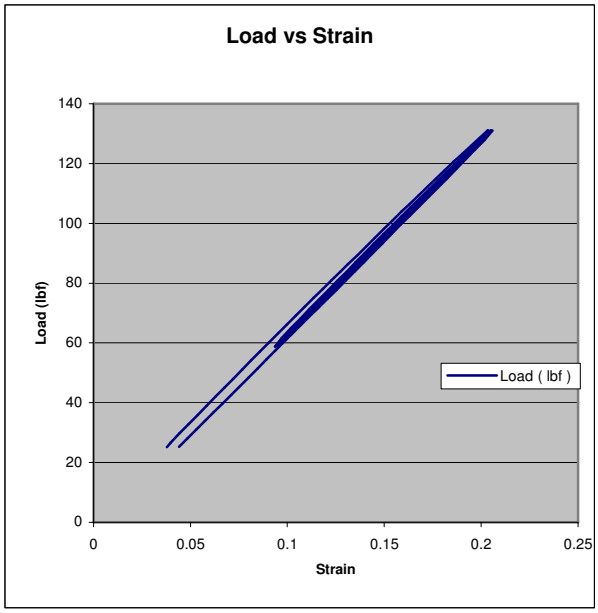

Figure 3. Example of load vs. strain response for the bulk testing.

TABLE 1. MATERIAL PROPERTIES

	Graphite	E-glass	Justification
Young's modulus 11 (GPa)	64	28	Measured value
Young's modulus 22 (GPa)	55	27	Measured value
Young's modulus 33 (GPa)	9.7	11	Micromechanics
Poisson's ratio 12	0.081	0.14	Measured value
Poisson's ratio 23	0.30	0.27	Micromechanics
Poisson's ratio 31	0.30	0.27	Micromechanics
Shear modulus 12 (GPa)	4.6	7.7	Measured value
Shear modulus 23 (GPa)	4.6	7.7	Estimate
Shear modulus 31 (GPa)	4.6	7.7	Estimate
CTE 11 ($°C^{-1}$)	1.e-6	8.e-6	Estimate
CTE 22 ($°C^{-1}$)	1.e-6	8.e-6	Estimate
CTE 33 ($°C^{-1}$)	3.e-5	3.e-5	Estimate

ENF Experiments

Mode II experiments were conducted employing the end-notched flexure (ENF) specimen design shown in Figure 4. Bimaterial beams are cut from a sheet composed of a graphite layer 0.074 ± 0.003 in thick and a glass layer 0.180 ± 0.003 in thick. The layers were oriented such that 0° off the rolling axis corresponded to the direction along the length of the ENF specimens. The sheet was cured at 350 °F

in the same manner as the tensile specimens. A thin Teflon film (0.002 in thick) was inserted between the two materials before curing so that the as-cut beams would have a precrack that extends from the left end of the beam to the location marked a_o in Figure 4. The bottom two pins are held fixed while the top pin is displaced downward at a rate of 0.001 in/s until the crack propagates and the applied load drops (see Figure 5).

The experiments were performed for two orientations: with the thin graphite layer on bottom (see Figure 4), and with the thin layer on top (not depicted). The dimensions for the specimen in Figure 4 are $L_1 = 1.101 \pm 0.001$ in, $L_2 = 1.953 \pm 0.001$ in, $L_3 = 2.077 \pm 0.001$ in, $a_o = 0.90 \pm 0.02$ in, and *width* = 1.001 $\pm$ *0.003* in. The specimen with the reversed orientation had the following measurements: $L_1 = 1.006 \pm 0.001$ in, $L_2 = 1.959 \pm 0.001$ in, $L_3 = 2.075 \pm 0.001$ in, $a_o = 0.99 \pm 0.02$ in, and *width* = 1.006 $\pm$ *0.003* in. The resolution on the force and displacement measurements were ± 0.3 lb and ± 0.0005 in, respectively.

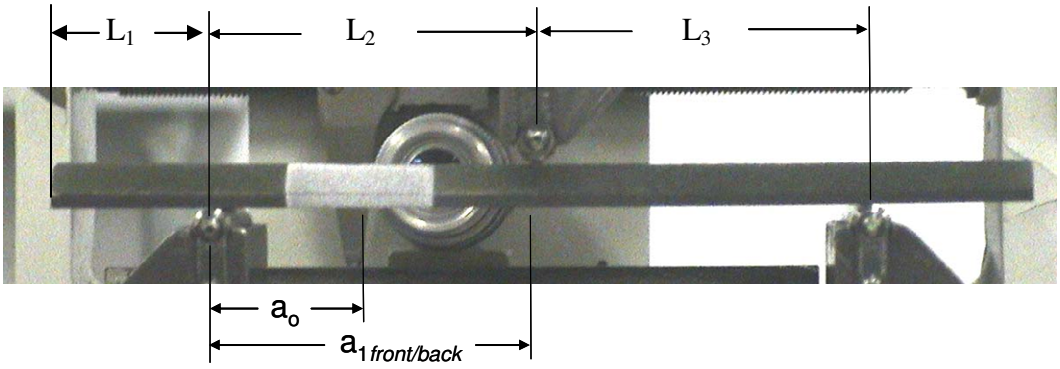

Figure 4. End-notched flexure specimen.

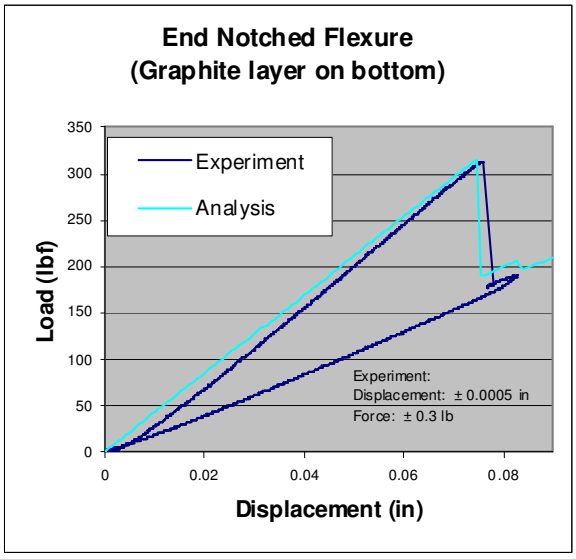

Figure 5. End-notched flexure results.

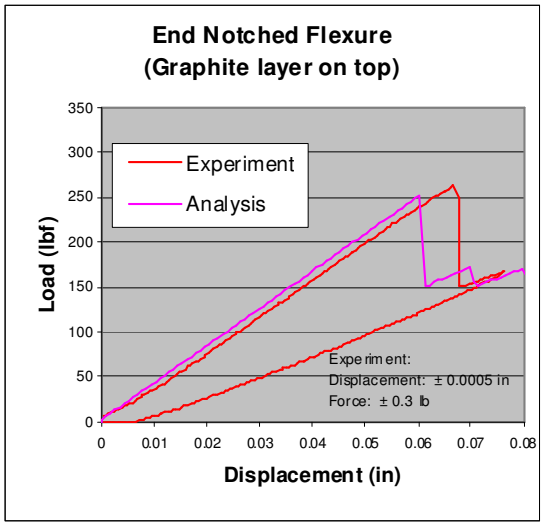

Figure 6. End-notched flexure results.

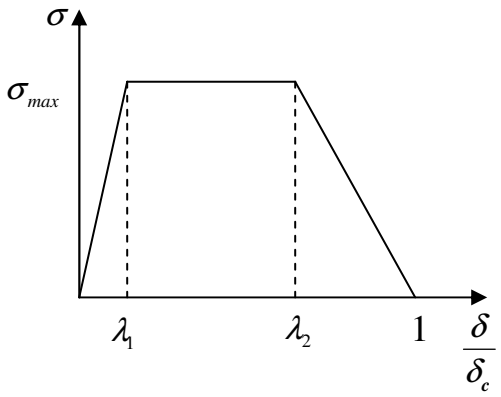

Figure 7. Traction-separation law for the cohesive zone model.

ENF SIMULATIONS

The meshes used for the simulations consisted of 14798 elements. The steel rollers were modeled with linear elasticity, whereas the composite beams were modeled using the linear elastic, orthotropic model described in [8] with the orthotropic material properties given in Table 1. The beams are attached by cohesive surface elements. Frictionless contact was used at the interface for the precracked region (Teflon film), as well as at the interfaces between the rollers and the beams. The cohesive surface elements obey the traction-separation law of Tvergaard and Hutchinson (see [5]), as shown in Figure 7. The critical energy-release rate is the area under the curve in Figure 7, where σ_{max} is the peak traction, δ is the separation, and δ_c is the critical separation, or characteristic length scale. Here, we assume the characteristic length scale is the same in both normal and

tangential directions. The parameters used in the simulations were as follows: σ_{max} = 31.6 MPa, $\lambda_1 = \lambda_2 = 0.5$, and δ_c = 0.0506 mm, for a critical energy-release rate of 800 J/m^2. The deformed mesh is shown in Figure 8 at the end of the simulation (after the crack has propagated to the middle of the specimen). The simulations included the effects of thermal mismatch by modeling the cool-down from the cure temperature (350 °F) to room temperature (70 °F) before loading is applied. The cohesive zone in the simulations extended across three elements for the coarsest mesh, giving a zone size of roughly 0.36 in.

The simulations matched the experimental results very well for both orientations (see Figures 5 and 6). The difference between the peak loads from the simulations and the experimental results for the two geometries were 1% and 4%, respectively. The difference in the load-displacement curves for the two orientations is due to the residual stress state that results from the specimen fabrication. The thin layer has a lower coefficient of thermal expansion (CTE) than the thick layer, so as the asymmetric beam is cooled to room temperature from the curing temperature, it curves slightly and puts the interface into shear. In the orientation depicted in Figure 4, the residual shear stresses from the CTE mismatch partially counteract against the stresses produced by loading, resulting in a higher failure load (Figure 5) as opposed to the case where the thin graphite layer is on top, such that the residual stresses enhance the shearing stresses introduced by the 3-point bending of the beam (Figure 6). This was verified by running the simulations for the two orientations without modeling the cool-down from the cure temperature, and the resulting load-displacement curves were nearly identical.

The crack propagation appears to be unstable for the ENF geometry with the dimensions used here. We neglected inertial effects by using a quasistatics code. This may account for the fact that the simulations underpredict the load drop that occurs as the crack propagates (see Figures 5 and 6). In the simulations, the specimens were loaded beyond the experimental displacements until further crack propagation was observed, and the corresponding load drops brought the load level down to that obtained in the experiments.

It should also be noted that the critical energy-release rate for the interface may differ from the value used here, since the Teflon film has a finite thickness and thus the precrack is not a sharp crack. Further experiments are being conducted on specimens for which the crack has already been extended away from the film before being used for end-notched flexure tests. When the corresponding simulations are performed, the effects of friction at the extended crack interface will need to be included.

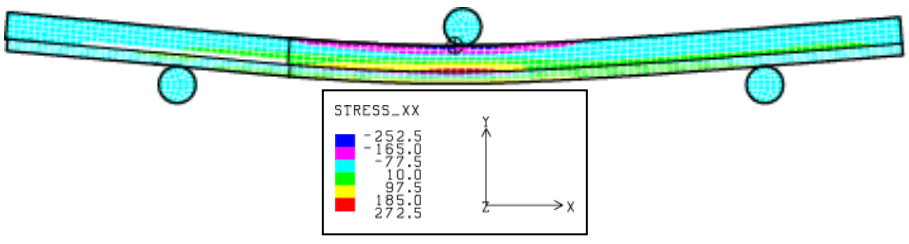

Figure 8. End-notched flexure specimen.

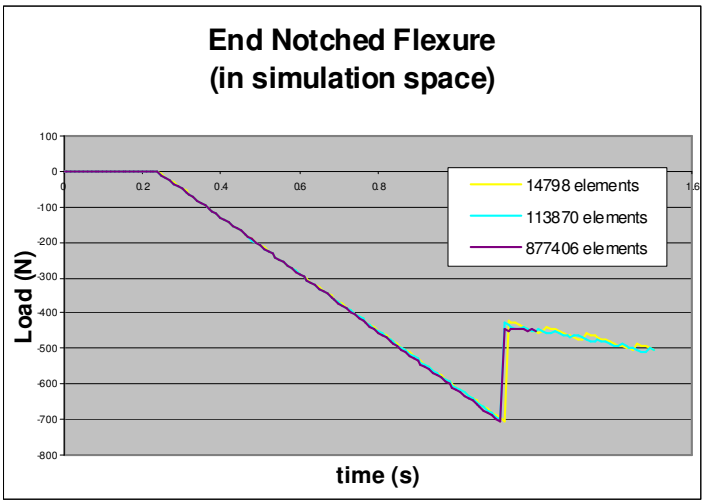

Figure 9. Sensitivity to mesh size.

To assess the mesh dependence of the simulations, we ran the ENF simulation with three different meshes, consisting of 14798, 113870, and 877406 elements (see Figure 9). The results did not differ significantly for any of the meshes.

SENSITIVITY ANALYSIS

For the end-notched flexure geometry in Figure 4, we have used Sandia's Design Analysis Kit for Optimization and Terascale Applications (DAKOTA) to run a sensitivity study with 37 geometric and material property parameters (see Table 2). Each parameter was given a range of +/- 5% of its nominal value. Latin Hypercube Sampling (LHS) methodology, which guarantees reasonably good coverage of the parameter space, was used to choose 800 sets of the 37 parameters. For each set of parameters, a finite-element simulation was performed and two response functions were calculated: f_1, which is the peak load in Newtons, and f_2, which is the initial specimen stiffness in N/m. The results from a smaller ensemble of simulations, for which only 42 parameter sets were chosen by the LHS method, are shown in Figure 10.

Both linear and quadratic model fits to each of two response objectives were obtained, and the sensitivity of each term was determined based on a statistical test for whether or not the coefficient of each term in the model fit is zero. Based on the 800 LHS runs, a least-squares fit was computed according to first a linear model,

$$f_m = a_0 + \sum_{n=1}^{N} a_n x_n \,, \tag{1}$$

where the x's are the $N = 37$ parameters, the a's (as well as the b's and c's below) are the model coefficients and $m = 1$ or 2 according to the particular response, and

then a quadratic model (using polynomials centered about the mean values $\bar{x}$ for the quadratic terms),

$$f_m = b_0 + \sum_{n=1}^{N} b_n x_n + \sum_{l=1}^{N} \sum_{k=1}^{i} c_{k,l} \left(x_k - \bar{x}_k \right) \left(x_l - \bar{x}_l \right), \tag{2}$$

where the latter has $(N^2 + 3N + 1)/2 = 741$ model coefficients. The coefficients are uniquely determined from a least-squares fit of the 800-run sample. The number of runs was chosen to modestly exceed the number of coefficients in a full quadratic model so that a possibly small number of outlying points would have relatively little influence on the least-squares fit to the data. The linear model yields a first estimate of the relative sensitivity of a response to each parameter, ignoring the effects of any parameter interactions, while the quadratic model gives an important indication of which parameter-interaction effects are potentially significant. The results from the linear fits are shown in Figure 11. For each plot, the y-axis represents the calculated value for the response function from the finite-element simulation, and the x-axis represents the predicted value based on the linear fit.

Sensitivity of a given response to each term is determined from the result of a test statistic that tests the (null) hypothesis that each coefficient, normalized by its statistical standard deviation, is zero. This test statistic is governed by a Student's *t*-distribution with $N - 1$ degrees of freedom (cf. [9], [10]). The *t*-distribution is a symmetric two-tailed probability distribution that is similar to, but generally broader and flatter than, a normal probability distribution and approaches a normal distribution in the large degrees-of-freedom limit (i.e., large sample size). If the value of the test statistic lies in either tail of the distribution, the null hypothesis fails, which means that the corresponding term in the model is likely to be significant and that the model displays a sensitivity to the parameter or parameter combination represented by that term. We remark that a zero coefficient in the model simply implies that the precise value of the corresponding parameter is unimportant; its nominal value is reflected in the model intercepts a_0 or b_0.

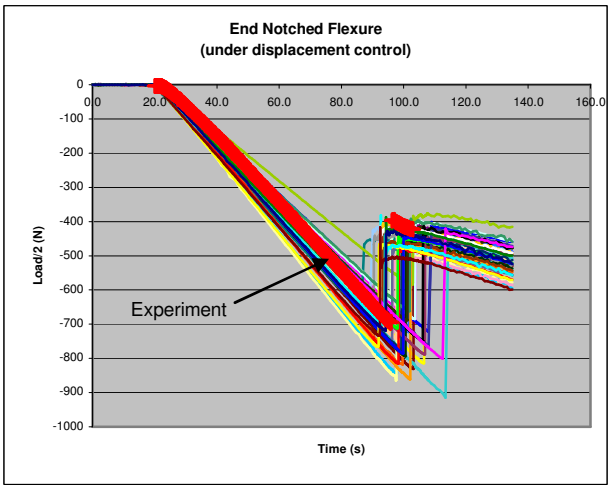

Figure 10. Ensemble from DAKOTA LHS study.

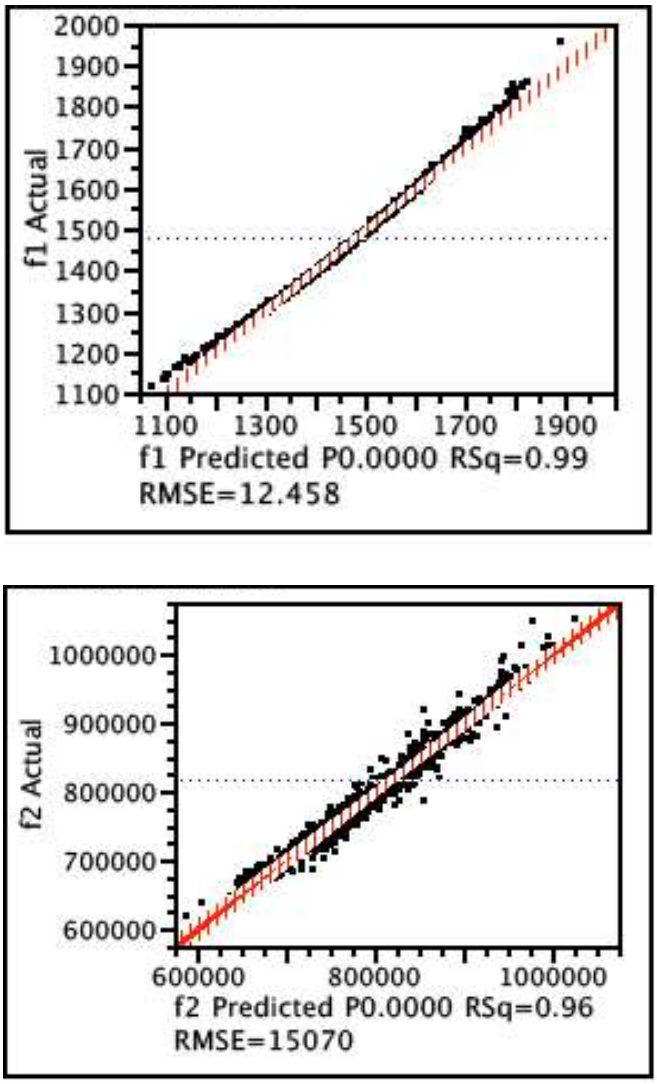

Figure 11. Linear fits for the two response functions from the LHS study.

Table 2 indicates the sensitivity results, obtained using the JMP® statistical software package, for the linear model for each of the two response functions (peak load and compliance) considered here. The columns "Prob > |*t*|" refer to how much of the *t*-distribution lies beyond the absolute value of the test statistic; i.e., a small value means that the value of the test statistic lies in one of the tails and that the corresponding term is therefore likely to be significant. A value less than 0.05 (less than 5% probability left in the tails) is usually regarded as sufficiently small for the *t*-test to fail. Values greater than 0.2 or so might be regarded as successful (i.e., the model is probably not sensitive to the value of the parameter associated with this term), whereas values between 0.05 and 0.2 might be an indication of moderate sensitivity.

TABLE 2. SENSITIVITY T-TEST RESULTS

Term	**f_1 prob > |t|**	**f_2 prob > |t|**
Intercept (a_0)	< .0001	< .0001
cure_temp	< .0001	0.5614
room_temp	0.1303	0.5031
CTE11_G	0.7966	0.6617
CTE22_G	0.4533	0.2176
CTE33_G	0.4152	0.2815
CTE11_E	< .0001	0.8442
CTE22_E	0.5667	0.7836
CTE33_E	0.0227	0.6741
YM11_G	0.0271	< .0001
YM22_G	0.8066	0.1070
YM33_G	0.0609	0.1685
PR12_G	0.8319	0.6878
PR23_G	0.7373	0.9830
PR31_G	0.3573	0.5217
SM12_G	0.2397	0.3210
SM23_G	0.4708	0.4713
SM31_G	0.3566	0.5254
YM11_E	< .0001	< .0001
YM22_E	0.7010	0.0776
YM33_E	0.8447	0.6400
PR12_E	0.9361	0.1873
PR23_E	0.0742	0.6131
PR31_E	0.0363	0.8099
SM12_E	0.0755	0.4638
SM23_E	0.4665	0.3808
SM31_E	0.7330	0.4767
lambda1	0.3498	0.0004
peak_traction	< .0001	< .0001
crit_energy_rel_rate	< .0001	< .0001
Length	0.0979	0.1878
Width	0.0000	0.0000
Thickness_G	< .0001	< .0001
Thickness_E	< .0001	< .0001
Precrack	0.0000	< .0001
L1	0.0000	< .0001
L2	< .0001	< .0001
L3	< .0001	< .0001

The results in Table 2 suggest, at least within the parameter range tested, that there are a number of sensitive and insensitive parameters with respect to both response functions, while in some instances, the type of response function

determines whether or not the value of a parameter is significant. For example, the last seven (geometric) parameters are clearly important for both response measures, but the precise length is of somewhat less importance. Some parameters, such as CTEaa_1, CTEbb_1, CTEcc_1, SMab_1, SMbc_1 and SMca_1, appear to have relatively small influence on both responses.

Some of the sensitivity results make intuitive sense; for example, the cure temperature affects the residual stresses and thus the failure load, but has little if any effect on the specimen stiffness. We also would expect the Young's moduli in the 11 direction to have a larger impact on the stiffness than the other orthotropic moduli, which is seen to be true. On the other hand, the stiffness response function should ideally not be sensitive to the cohesive parameters, although similar behavior has been noted by others (see de Moura [1] and Blackman et al. [11]). This finding may mean that the initial stiffness of the traction-separation law needs to be increased. Unfortunately, this leads to numerical issues for the finite element solver.

One benefit to the sensitivity analysis is that it helps determine what further experiments may be necessary. The estimated shear moduli (see Table 1) do not appear to influence the responses significantly, so it may not be worth the cost to determine more accurate values. Conversely, a couple of the coefficients of thermal expansion have significant sensitivities, so it may be desirable to perform additional experiments to accurately determine their values.

There are too many interaction terms in the quadratic fit to present here, but the results from the quadratic fit will be used to determine the most significant parameter-interaction effects. The results from the sensitivity analysis will also be used to reduce the number of parameters used in uncertainty analysis.

CONCLUSIONS

Cohesive surface elements were utilized to model mode II failure for the end-notched flexure geometry. Experiments were conducted to determine the bulk properties, and end-notched flexure experiments were performed using bimaterial composite specimens. The finite-element simulations agreed well with the experimental results.

A sensitivity analysis study was performed for 37 uncertain geometric and material property parameters, each given a range of +/-5% its nominal value. DAKOTA's Latin Hypercube Sampling method was used to generate an ensemble of 800 Adagio simulations, from which maximum load and compliance responses of the test specimen were computed. Linear and quadratic model fits were performed for each of the response functions. The sensitivity of each parameter was determined based on a statistical test for a null hypothesis.

Follow-on uncertainty quantification studies using Adagio and DAKOTA will be performed in the future. Temperature and rate effects are also being studied, and experiments with mode I and mixed-mode failure will be conducted.

ACKNOWLEDGEMENT

This work was performed at Sandia National Laboratories. Sandia is a multiprogram laboratory operated by Sandia Corporation, a Lockheed Martin Company, for the United States Department of Energy under contract DEAC04-94AL85000.

REFERENCES

1. de Moura, M. F. S. F., 2006. "Numerical Simulation of the ENF Test for the Mode-II Fracture Characterization of Bonded Joints," *J. Adhesion Sci. Technol.*, Vol. 20, no.1, pp.37-52.
2. Iannucci, L., 2006. "Dynamic Delamination Modelling Using Interface Elements," *Computers & Structures* Vol. 84, Issues 15-16, pp. 1029-1048.
3. Mi, Y., M. A. Crisfield, G. A. O. Davies and H. B. Hellweg, 1998. "Progressive Delamination Using Interface Elements," *Journal of Composite Materials*; Vol. 32, pp.1246-1272.
4. Liu, S., Y. Mei, and T. Y. Wu, 1995. "Bimaterial Interfacial Crack Growth as a Function of Mode-Mixity," *IEEE Transactions - Part A*, Vol. 18, No. 3, pp.618-626.
5. Tvergaard, V., and J. W. Hutchinson, 1996. "On the Toughness of Ductile Adhesive Joints," *J. Mech. Phys. Solids,* Vol. 44, No. 5, pp. 789-800.
6. Anderson, T.L., 2005. *Fracture Mechanics*, 3rd edition, CRC Press, Florida.
7. ASTM Standards and Literature References for Composite Materials, 2nd ed, 1990.
8. Hammerand, D. C., 2004. "Laminated Composites Modeling in ADAGIO/PRESTO," Sandia Report SAND2004-2143, Sandia National Laboratories, Albuquerque, NM.
9. Montgomery, D. C., 2005. *Design and Analysis of Experiments*, Wiley.
10. Wackerly, D. D., W. Mendenhall III and R. L. Schaeffer, 2002. *Mathematical Statistics with Applications*, Duxbury/Thomson Learning, Pacific Grove, CA.
11. Blackman, B.R.K., A.J. Kinloch, M. Paraschi, 2005. "The determination of the mode II adhesive fracture resistance, G_{IIC}, of structural adhesive joints: an effective crack length approach," Engineering Fracture Mechanics 72. pp. 877–897.